Construction and Building Materials 308 (2021) 125036

Contents lists available at ScienceDirect

Construction and Building Materials

journal homepage: www.elsevier.com/locate/conbuildmat

A numerical anatomy-based modelling of bamboo microstructure

Layth S. Al-Rukaibawi [a,*], Sadik L. Omairey [b], György Károlyi [c]

[a] Department of Structural Engineering, Budapest University of Technology and Economics, Műegyetem rkp. 3, 1111 Budapest, Hungary
[b] Brunel Composites Centre, College of Engineering, Design and Physical Sciences, Brunel University London, London, UK
[c] Institute of Nuclear Techniques, Budapest University of Technology and Economics, Műegyetem rkp. 3, 1111 Budapest, Hungary

ARTICLE INFO

Keywords:
Moso Bamboo
RVE
Homogenisation
Natural Fibre
Bio-Based Composites
Sustainability

ABSTRACT

Bamboo has attracted considerable recent interest in sustainable buildings as the fastest-growing natural material retaining mechanical properties similar to structural wood while being an effective CO_2 absorber during its growth. Previous efforts to estimate bamboo material properties and their behaviour using homogenisation techniques used simplified assumptions on the geometry of the inhomogeneous microstructure, hence these methods failed to account for the different homogenised material properties in the directions lateral to the bamboo culm. This study presents a novel anatomy-based numerical bamboo microstructure analysis that accurately represents the geometrical features of the material, leading to a transversely anisotropic effective material model. We compare the resulting effective elastic properties to those obtained with state-of-the-art numerical and analytical approaches found in the literature. It is concluded that our anatomy-based representative volume element provides a better understanding of the material microstructure and its corresponding effective stiffness properties in the longitudinal and lateral directions.

1. Introduction

Finding sustainable biological construction materials have gained significant recent interest [1,2]. One of these materials is bamboo, a fast-growing plant with mechanical properties similar to those of structural wood products [3], while being an effective CO_2 absorber compared with other materials such as plastics, metal and concrete [4]. Morphologically, the bamboo plant contains two major components, the rhizomes and the culms. The rhizome stores the nutrients necessary for growth and secures the plant underground. The culm is the upper part of bamboo containing mostly wood-like material [5]. It can be considered as a hollow cylinder or tapered tube divided into several internodes separated by diaphragms or nodes (see Fig. 1a). The bottom segment of the culm has the largest diameter and wall thickness, but the average internode length is lower at the bottom in comparison with upper segments of bamboo. These characteristics make the base of the culm suitable to carry considerable compressive loads. The diameter and thickness of the wall increase from the top to the bottom [6–8].

Bamboo is considered a composite material reinforced by vascular bundles and parenchyma matrix as seen in Fig. 1. The vascular bundles are composed of unidirectional stiff sclerenchyma-cells (fibre bundles) of approximately 21–40% gross volume fraction [8,10–14]; this includes approximately 5–8% conductive tissues (tubes of vessels) transporting nutrients and water vertically along the culm wall. The vascular bundles are embedded in the spongy tissue called parenchyma cells (matrix); this occupies the remaining region, see Fig. 1(b). The distribution of fibre bundles is denser in the outer region of the culm wall (about 60 % volume fraction) compared with the inner region (about 10–15 %) [8,11,13]. As a result of this radial increase of the amount of fibres from the inside to the outside [8,12,13], the strength of the outer wall layers is higher than that of the inner layers [11]. Despite the obvious taper in culm geometry, the mechanical properties of the culm are relatively uniform from the ground up [15].

Although there are over 1600 species of bamboo, this study employs data of Moso bamboo (Phyllostachys edulis), because in recent years numerous experimental investigations were conducted on the structural features of this type of bamboo. For instance, Shao et al. [13] quantitatively analysed the variation of fibre area in connection with Moso bamboo tensile properties across the radial thickness of the internodes. They reported the tensile strength and elastic modulus of fibre bundles to be around 480 MPa and 34 GPa, respectively. Li and Shen [14] studied the elastic modulus longitudinal to the grain at different locations (base, bottom, and top) of the Moso culm. They proposed empirical equations to compute stiffness, stress, and volume fractions. Tan et al.

* Corresponding author.
E-mail addresses: syyd.salman.al-rukaibawi@epito.bme.hu (L.S. Al-Rukaibawi), karolyi@reak.bme.hu (G. Károlyi).

https://doi.org/10.1016/j.conbuildmat.2021.125036
Received 18 April 2021; Received in revised form 21 September 2021; Accepted 22 September 2021
Available online 13 October 2021

[16] investigated the crack growth and toughening mechanisms of Moso bamboo culm experimentally and numerically. García et al. [17] studied the transverse elastic modulus using ring specimens. Another study by Sharma et al. [18] determined transverse mechanical properties of full-culm bamboo. While Dixon and Gibson [10] measured several elastic parameters of Moso bamboo quantitatively and measured the elastic modulus of fibre bundles to be 40 GPa, and that of the parenchyma matrix to be 5 GPa. In conclusion, these studies mainly focused on estimating the strength and homogenised moduli in either longitudinal or transversal directions.

On the other hand, studies such as Liu et al. [19] and Shang et al. [20] applied advanced optical imaging, namely, confocal laser scanning microscopy to measure the graded volume fraction accurately for the vascular bundles and bamboo strips across the culm wall, while the graded elastic modulus and tensile strength through the thickness of the culm wall was captured accurately in tensile tests of single vascular bundles. Liu et al. [19] reported the tensile strength and the elastic modulus of fibre bundles in the inner layer of the culm to be around 101 MPa and 7 GPa, respectively, and those at the outer layer to be approximately 294 MPa and 30 GPa, respectively. While Shang et al. [20] reported the tensile strength and elastic modulus of the inner layer to be around 458 MPa and 29 GPa, respectively, and those of the outer layer to be 709 MPa and 44 GPa, respectively. The effect of fibre gradient on gross culm stiffness is reported to be marginal for P. edulis (about 5 %) which is explained as a consequence of a thin-walled characteristic [21], see also [22].

Although many factors including moisture content, degree of lignification related to age at harvest, etc. affect the mechanical properties [23], the deviation between the aforementioned experimental results highlights the need to understand the function of structural features, such as the complex microstructural shapes and gradient material distribution on the performance of bamboo.

To understand this better, many studies focused on closed-form analytical micromechanics equations and numerical modelling of bamboo fibres. For instance, Li and Shen [14] employed an analytical model based on the rule of mixture (ROM) to predict the effective properties of bamboo vascular bundles. While Lee et al. [24] computed analytically the distribution of the elastic modulus of Moso bamboo based on three distribution functions: namely, the linear, power, and exponential functions. While Wang et al. [25] proposed an analytical model to predict the gradient of the material properties and the anisotropy based on the assumption of the deformation gradient tensor and found that the simple ROM model is an inaccurate method for predicting stiffness and elastic modulus of bamboo fibres. Zhao et al. [26] proposed using more sophisticated and yet simple micro-mechanical models, the Halpin–Tsai (H–T) equations and the Mori–Tanaka (M−T).

On the other hand, a numerical solution instead of analytical was proposed by Silva et al. [27]. This study modelled bamboo as a functionally graded material. They employed graded finite elements to the bamboo unit cell to capture the spatially varying stiffness properties by means of a generalised isoparametric formulation. Additionally, a recent study by Cui et al. [28] adapted a computational homogenisation approach based on a representative volume element (RVE) to study the mechanical response of a bamboo culm under axial compressive load, and systematically investigated bamboo's hierarchical structural features. This study used a simplified representation of bamboo's microstructure, using RVE containing two phases, fibre and matrix; the fibre was represented by either squared or circular shape for a given volume fraction.

The above analytical and numerical-based models simplified the complex microstructure of bamboo's culm (i.e., the vascular bundles and parenchyma matrix, see Fig. 1(b)) into normalised fibre/matrix regions, mainly for simplification and compatibility with existing numerical models and analytical equations without accounting for the effect of the complex microstructure on the performance of the culm. Therefore, this study presents a novel numerical anatomy-based modelling strategy for the bamboo microstructure, which enables investigating the effect of the complex microstructure on the homogenised properties of the culm. This proposed anatomy-based RVEs captures the geometrical features of the vascular bundles and parenchyma matrix at four different layers of the culm wall. These RVEs are then analysed to estimate the stiffness properties by imposing periodic boundary conditions within a finite element analysis (FEA) based RVE homogenisation method. Additionally, to verify and establish the importance of the detailed microstructure modelling and analysis, the

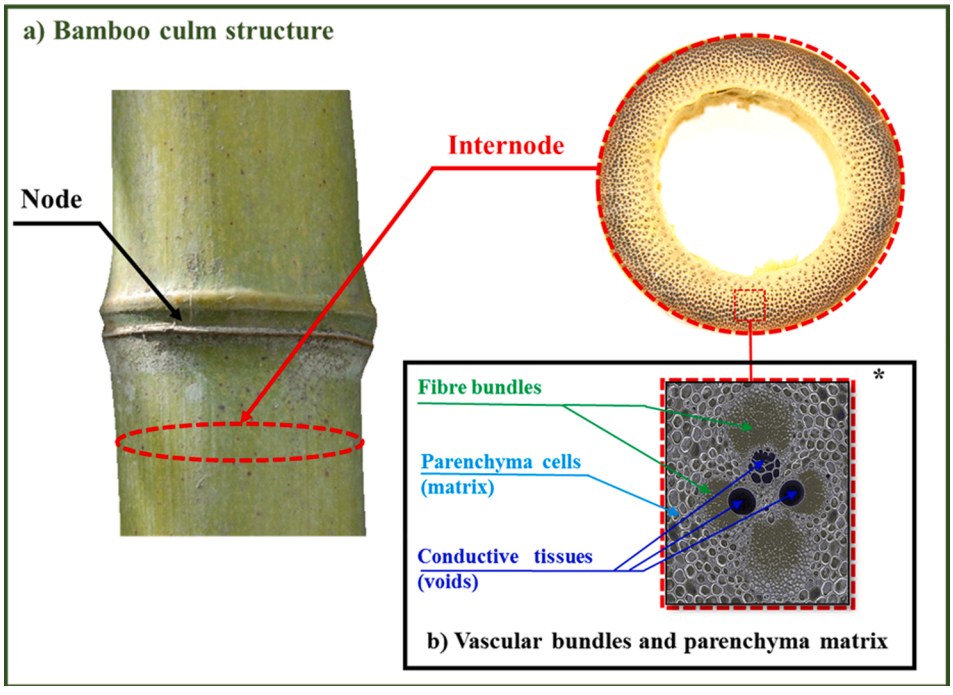

Fig. 1. Characteristic bamboo structure with a) culm section and b) vascular bundles and parenchyma matrix. The microscopic image is taken from [9].

effective elastic properties obtained from the anatomy-based RVE approach are compared with single fibre RVE representation (single fibre within a matrix phase) and several analytical homogenisation methods.

The remainder of this paper is structured as follows: Section 2 describes the configuration employed to represent bamboo microstructure with fibres (vascular bundles) and matrix (parenchyma). The review of five analytical approaches and homogenisation-based constitutive methods in terms of the effective elastic properties are briefly described in Section 3. Subsequently, Section 4 presents in detail two sophisticated numerical homogenisation models: the single fibre RVE and an anatomy-based model based on representative volume elements. The obtained effective elastic properties from the analytical models and the two numerical RVE's are compared to the available experimental longitudinal elastic modulus and further discussed with the aid of elastic strain energy in Section 5. Finally, the main conclusions and future work are presented in Section 6.

2. Elastic properties of bamboo

Moso bamboo can be considered as a multi-layered orthotropic material with high strength parallel to the stem (axis × or axis 1 below) and low strength in the transversal directions. At the micro-scale, the elastic properties of each bamboo layer depend on the elastic properties and volume fractions of two phases: vascular bundles of fibres surrounded by a matrix of parenchyma. The bamboo fibres are considered to be continuous and long. We assume each phase of the Moso bamboo to be perfectly bonded, linearly elastic and isotropic solid, these assumptions are similar to those applied in other studies [29,30]. The elastic properties of the bamboo culm vary along the radius (axis *y* or axis 2 below denotes radial direction, while axis z or 3 denotes the tangential direction). For simplicity, we assume four different radial layers with different elastic modulus decreasing radially from the outer layer towards the inner layer. We call them the inner, the middle-1, the middle-2 and the outer layer.

Table 1 summarises the elastic properties that we use in this paper for the vascular bundles and parenchyma matrix sub-regions in each layer.

3. Analytical homogenisation approach

In this section, we review five well-known analytical homogenisation-based constitutive methods for unidirectional fibre reinforced composites. These approaches are often used in the micro-mechanical analysis because they are fast, easy to implement and require minimal computational resources. The main theme of the analytical homogenisation is the development of a representative volume element (RVE) to represent the heterogeneous materials made of constituent phases. We apply these methods to estimate the stiffness properties of bamboo which can be considered a unidirectional fibre reinforced composite material.

Table 1
Elastic properties for Moso bamboo fibres (*f*) and matrix (*m*).

Elastic constants	Young's modulus (GPa)		Poisson's ratio		Volume fractions (%)	
	E_f	E_m	ν_f	ν_m	V_f	V_m
Inner	54.19	2.16	0.28	0.34	8.53	91.47
Middle-1	55.53	2.16	0.28	0.34	12.69	87.31
Middle-2	57.60	2.16	0.28	0.34	21.86	78.14
Outer	64.09	2.16	0.28	0.34	47.2	52.8
Source of data	[12]	[16]	[31]	[25]	[12]	[*]

[*] Calculated as (1-V_f).

3.1. Rule of mixture (ROM) and inverse ROM models

Rule of mixture (ROM) and inverse ROM are simple models widely known as *iso*-strain Voigt [32] and *iso*-stress Reuss [33] models, respectively, primarily applied for polycrystals. The Voigt model is based on the assumption that the strains in the constituents are constant [32]. In the same manner, the Reuss model is based on the assumption that the stresses are constant [33]. The former approach is used for axial loading while the latter is used for transverse loading. The analytical relations for the Voigt model are given as

$$\mathrm{E}_{11} = \mathrm{V_f E}^{\mathrm{f}}_{11} + V_m \mathrm{E}^{\mathrm{m}}_{11}, \quad \upsilon_{12} = V_f \upsilon^f_{12} + V_m \upsilon^m_{12}. \tag{1}$$

Here, the longitudinal elastic modulus E_{11} and Poisson's ratioυ_{12} are computed as the weighted average of those in the matrix (E^{m}_{11}, υ^m_{12}) and the fibres (E^{f}_{11}, υ^f_{12}). Averaging is taken with respect to the volume fractions of the matrix and the fibres (V_m, V_f, respectively).

For the Reuss model, we have

$$E_{22} = \frac{E^f E^m}{E^m V_f + E^f V_m}, \quad G_{12} = \frac{G^f G^m}{G^m V_f + G^f V_m}. \tag{2}$$

Here, the transverse elastic modulus E_{22} and the shear elastic modulus G_{12} can be computed as the weighted average of those in the matrix (E^{m}_{11}, G^m_{12}) and the fibres (E^{f}_{11}, G^f_{12}). Averaging is taken with respect to the volume fractions of the matrix and the fibres (V_m, V_f, respectively).

3.2. Improved rule of mixture (IROM) model

This model is an improved version of ROM using three-dimensional orthotropic stress–strain relations developed by Qing and Mishnaevsky [34]. This approach considers two continuity conditions: on the one hand, the constraint of the compatibility of deformations and displacements at the interface of the fibre and the matrix, and, on the other hand, the equilibrium of stresses at phase boundaries. Using these continuity conditions, we managed to derive and write analytical relations for the elastic moduli and Poisson's ratios for fibres and matrix in three principal directions: longitudinal, radial, and tangential, using the symbolic mathematical computing software Maple (version 2020). See Supplementary Material A for the complete set of equations.

3.3. Halpin-Tsai (H-T) model

This model is a semi-empirical model based on the self-consistent model developed by Hill [35]. It is also known as an improved ROM applied extensively to predict transverse Young's modulus and in-plane shear modulus [26]. The model tends to correct the mismatch of stresses in fibres and matrix by introducing a semi-empirical parameter η and a reinforcing factor ξ. Young's modulus E_{11} and Poisson's ratio ν_{12} can be predicted as in the ROM model, see (1). The transverse Young's modulus is

$$E_{22} = \left(\frac{1+\zeta\eta V_f}{1-\eta V_f}\right) E^m \tag{3}$$

where $\eta = \frac{E^f - E^m}{E^f + \zeta E^m}$, and $\zeta = 2$ for circular shape fibres in a square array with volume fraction ≤ 0.5 [36]. The in-plane shear modulus is

$$G_{12} = \left(\frac{1+\zeta\eta V_f}{1-\eta V_f}\right) G^m \tag{4}$$

where $\eta = \frac{G^f - G^m}{G^f + \zeta G^m}$, and $\zeta = 1$ for circular shape fibres in a square array. The out-of-plane shear modulus is

$$G_{23} = \left(\frac{1+\zeta\eta V_f}{1-\eta V_f}\right) G^m \tag{5}$$

where $\eta = \frac{G^f - G^m}{G^f + \zeta G^m}$, and $\zeta = \frac{1+\nu^m}{3-\nu^m-4(\nu^m)^2}$ for circular shape fibres in a square array.

3.4. Chamis model

This model is widely used to predict matrix-fibre elastic properties [37]. Chamis assumed that both fibre and matrix are linearly elastic, and the fibres are spaced periodically in square or hexagonally packed arrays. Hence, this model cannot consider the changes in geometrical configurations. Its formulation provides all five independent elastic properties for the composite of matrix and fibre. Elastic modulus E_{11} and the Poisson's ratio ν_{12} can be estimated as in the ROM model, see (1). The transverse Young's modulus is

$$E_{22} = E_{33} = \frac{E^m}{1 - \sqrt{V_f}\left(1 - \frac{E^m}{E^f}\right)} \tag{6}$$

In-plane shear modulus G_{12} and out-of-plane shear moduli G_{23} and G_{13} are

$$G_{12} = G_{13} = G_{23} = \frac{G^m}{1 - \sqrt{V_f}\left(1 - \frac{G^m}{G^f}\right)} \tag{7}$$

The minor Poisson's ratio is

$$\nu_{23} = \frac{E_{22}}{2G_{23}} - 1 \tag{8}$$

3.5. Mori-Tanaka (M−T) model

This model, developed by Mori and Tanaka based on the Eshelby average stress tensor in the matrix [30] is well-known as an exact elastic homogenisation technique. It is considered as an accurate estimate for fibre–matrix stiffness properties. It has a wide range of applications for many different types of composite materials. The central assumption of this method is that composites containing two or more phases are modelled in such a way that the average strain of randomly aligned fibres with an elliptical shape having low to moderate volume fractions can be approximated as an inclusion embedded in an infinite matrix of average strain. Hosseini et al. [38] have given the explicit relations in terms of the bulk modulus K of the homogenised bamboo fibres and matrix:

$$K = \frac{E^m\left[E^m V_m + 2K_f(1+\nu_m)\left(1 + V^f(1-2\nu_m)\right)\right]}{2(1+\nu_m)\left[E^m\left(1+V^f-2\nu_m\right) + 2V^m K_f\left(1-\nu_m-2\nu_m^2\right)\right]} \tag{9}$$

The longitudinal Young's modulus is

$$E_{11} = \left(\frac{E^f}{E^m}V_f + V_m\right)E^m + \frac{2V_f V_m\left(\nu_f - \nu_m\right)^2 \frac{E^f}{E^m}E^m}{V_m(1+\nu_m)(1-2\nu_f) + \frac{E^f}{E^m}(1+\nu_m)(1+V_f(1-2\nu_m))} \tag{10}$$

The major Poisson's ratio is

$$\nu_{12} = \frac{2V_f\frac{E^f}{E^m}(1-\nu_m^2)\nu_f + V_m\nu_m[(1+\nu_f)(1-2\nu_f) + \frac{E^f}{E^m}(1+\nu_m)]}{2V_f\frac{E^f}{E^m}(1-\nu_m^2) + V_m[(1+\nu_f)(1-2\nu_f) + \frac{E^f}{E^m}(1+\nu_m)]} \tag{11}$$

The transverse Young's modulus is

$$E_{22} = \frac{4KG_{23}}{(K + qG_{23})} \tag{12}$$

with $q = 1 + \frac{4K\nu_{12}^2}{E_{11}}$. The minor Poisson's ratio is

$$\nu_{23} = \frac{(K - qG_{23})}{(K + qG_{23})}. \tag{13}$$

The in-plane shear modulus is

$$G_{12} = \frac{\left[\frac{E^f}{E^m}\left(1+V_f\right)(1+\nu_m) + \left(1-V_f\right)\left(1+\nu_f\right)\right]E^m}{2(1+\nu_m)\left[\frac{E^f}{E^m}\left(1-V_f\right)(1+\nu_m) + \left(1+V_f\right)\left(1+\nu_f\right)\right]} \tag{14}$$

The out-of-plane shear modulus is

$$G_{23} = \frac{\left[\left(1-V_f\right)\left(1+\nu_f\right) + \frac{E^f}{E^m}(1+\nu_m)\left(V_f+3-4\nu_m\right)\right]}{2(1+\nu_m)\{[(1-V_f)(1+\nu_m)(3-4\nu_m)\frac{E^f}{E^m} + (1+V_f) + [1+V_f(3-4\nu_m)]\}}. \tag{15}$$

As it has been shown, the above analytical micromechanics methods are strictly valid for inclusions (fibres) with isotropic or transversely isotropic properties having a rounded circular shape. However, bamboo has complex fibre shapes with vessels. Hence, it is expected that these models cannot accurately account for the effect of microstructure in the transverse direction. To some extent, some of these methods are not appropriate for estimating the overall stiffness of bamboo, such as the Voigt and Reuss (ROM) models [14], yet it is presented here as it forms the base deriving the development of other methods. Also, bamboo does not have transversal isotropy, whereas current models are all designed for transversely isotropic effective material models. Therefore, to accommodate for the effect of geometrical variations of bamboo constituents at the micro-scale level, an FEA-based numerical RVE homogenisation approach has been proposed in the following section.

4. The numerical RVE homogenisation approach

The RVE homogenisation method imposes uniform strains on a micro-scale RVE to numerically compute the effective elastic properties. The RVE should be selected and modelled such that it provides a sufficient representation of the material at higher scales. This method is widely used for composite materials for its clear mechanical conception and simplicity.

The numerical RVE homogenisation assumes that the average stiffness properties of an RVE are equal to the average properties of the particular heterogeneous material. Hence, the average stresses $\bar{\sigma}$ and strains $\bar{\varepsilon}$ in an RVE are defined as:

$$\bar{\sigma} = \frac{1}{V}\int_V \sigma dV, \quad \bar{\varepsilon} = \frac{1}{V}\int_V \varepsilon dV \tag{16}$$

where V is the volume of the RVE. In order to evaluate the corresponding effective homogenised stiffness tensor C_{ij}, the above average stress and the corresponding average strain are evaluated with the desired boundary conditions, then:

$$C_{ij} = \frac{\sigma_{ij}}{\varepsilon_{ij}} \tag{17}$$

Since the RVE homogenisation method requires the implementation of uniform strains on the RVE to compute the effective elastic properties, periodic boundary conditions are applied, which ensure that the RVE's deformed external surfaces remain periodic [39–41]. The RVE homogenisation method can be implemented using commercial FEA software.

For a transversely isotropic material, five independent parameters remain in the elastic tensor. The planar boundary surfaces of RVEs remain planes under imposed longitudinal and transverse deformations or displacements. However, bamboo is an orthotropic material meaning that it requires nine independent parameters in its elastic tensor. In this case, the boundary surfaces can distort and no longer remain planes under imposed shear strain. To achieve periodic boundary conditions, one requires nodal displacement degrees of freedom (DoF) based on the concept of unified periodic RVE homogenisation [42]. Following the work of Omairey et al. [43], the nodal sets of DoF for six elementary loadings (three for elastic moduli with the corresponding Poisson's ratio, and three for shear moduli) are constructed using linear constraint

equations and displacement boundary conditions within ABAQUS subroutine. For a detailed elaboration on them, see [43].

The use of FEA-based homogenisation involves identifying an RVE. One of its first definitions states that it should contain a sufficient number of inclusions and be typical of the mixture on average [44]. As the homogenised properties of the RVE will represent the properties on larger scales, it is important to capture it accurately to ensure accurate representation of the material. In the literature, this was done using an RVE that contain two phases, a fibre surrounded by matrix; this implementation is adopted in Sec. 4.1 of this study for comparison and validation. On the other hand, this study proposes having this representation in the form of an anatomy-based RVE that mimics bamboo's microstructure; this configuration is detailed in Sec. 4.2.

To conduct numerical homogenisation for the two RVE configurations, EasyPBC tool [43] is used to estimate the stiffness properties of the modelled RVEs, as it offers the freedom to create a wider range of geometries in the pre-processing and extended access to the post-processing analysis data. EasyPBC tool implements homogenisation by numerically imposing uniform strains and deformations on the RVE to obtain the overall engineering moduli as shown in Fig. 2 for the proposed anatomy-based RVE.

4.1. Single- fibre RVE

The structure of Moso bamboo cross-section is heterogeneous and functionally graded. For the single-fibre RVE model, fibre shape effect is omitted and assumed to have of circular cross-section with square packing. The configuration of this transversely isotropic RVE is shown in Fig. 3. The fibres in this model are oriented in the direction of the x-axis (direction 1) and are considered to be continuous. It is assumed that the phases of the Moso bamboo to be perfectly bonded, linearly elastic and isotropic solid. These assumptions are similar to those applied in Refs. [29,30].

The model is created in ABAQUS FEA software and analysed by EasyPBC homogenisation tool, having a length (L), width (W), and thickness (t) of 1 mm along the longitudinal x-axis, tangential z-axis, and radial direction y-axis, respectively as shown in Fig. 3. The RVE model is discretised using hexahedral elements with structured meshing technique. Three-dimensional 20-node quadratic brick elements with reduce integration (C3D20R) are adopted for meshing to efficiently capture bending and buckling within the linearly elastic range [28]. The mesh size of 0.04 mm is chosen, resulting in the number of mesh elements 19,150, 19,175, 18,525 and 19,375 from inner towards outer layers, respectively. This resolution was found to be fine enough to achieve convergence of the solutions.

4.2. Anatomy-based RVE

To reflect a more realistic bamboo microstructure, this study introduces a new anatomy-based micromechanical model. The vascular bundles of Moso bamboo are built up from three constituents; fibre bundles of circular and crescent cross-sectional shapes which are surrounded by a matrix of parenchyma cells, and hollow tubes of vessels that transfer water and nutrients. These fibre bundles are distributed densely in the outer region of the culm wall and sparsely in the inner region [25,45,46]. To reflect a more realistic bamboo microstructure, this study introduces a new anatomy-based micromechanical RVE model that accounts for all of these constituents at the micro level.

Shao and Wang [47] have made an idealisation of bamboo vascular bundles consisting of semi-circular fiber bundles and squared vessels, in which they studied the energy absorbing mechanism of Moso bamboo under various damage patterns. As a step forward, this study reconstructs an anatomy-based computational model from four scanning electron microscopic images of specimens of bamboo internodes studied by Dixon and Gibson [10] and made publicly available through DSpace [9]. Based on these images, commercial CAD software was used to

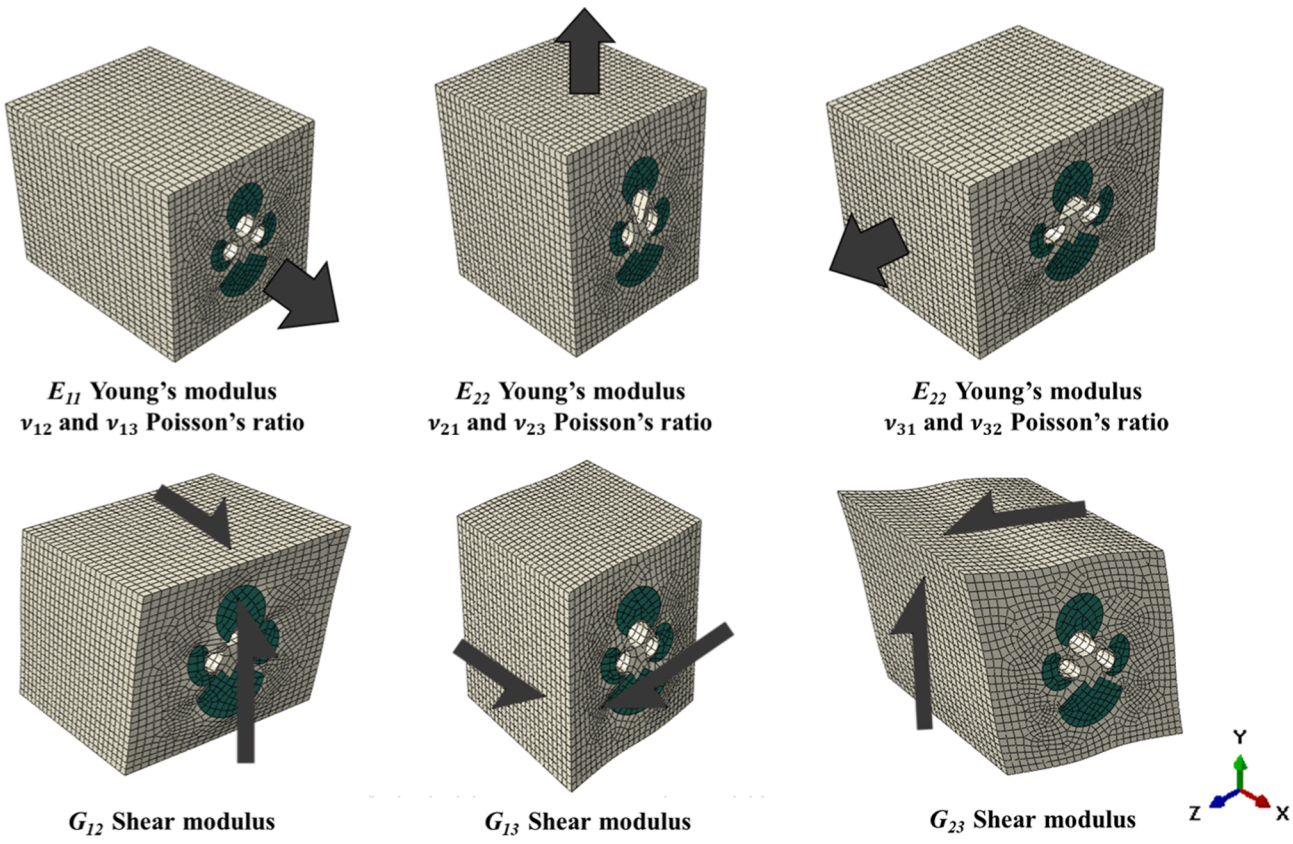

Fig. 2. Schematic representation of six displacement boundary conditions used to obtain the elasticity parameters indicated for each case.

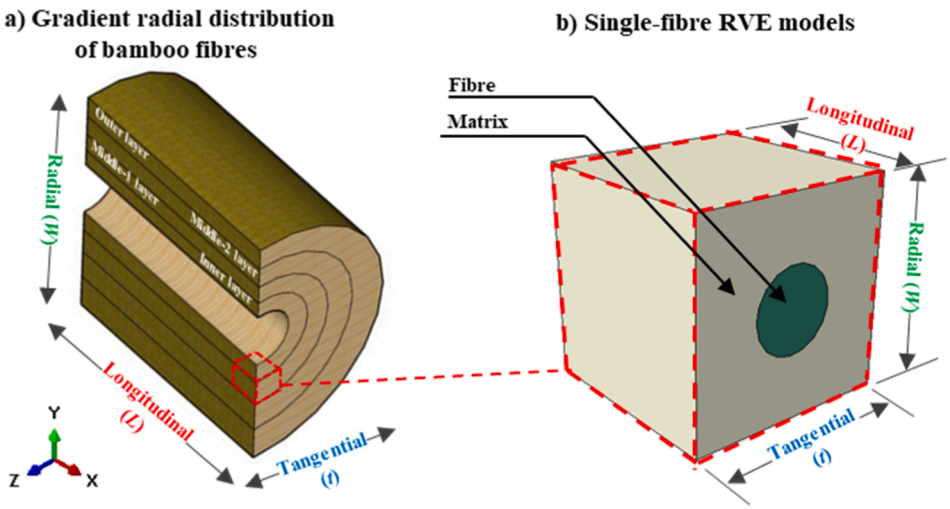

Fig. 3. Moso bamboo composite and its single-fibre RVE. (a) Gradient radial distribution of bamboo fibres. (b) The schematic square array around the circular fibre bundles with the geometrical parameters of RVEs that are different in each layer shown in (a). We set side lengths W, L and t to be constant (1 mm) and vary the fibre bundle (green) diameter d between 0.33, 0.4, 0.52 and 0.77 mm from the inner layer outwards to account for proper fibre distribution. (For interpretation of the references to colour in this figure legend, the reader is referred to the web version of this article.)

construct three-dimensional RVE cubes that capture the native structure of bamboo vascular bundles in each layer from the inner to the outer layers. The generated anatomy-based model consists of fibre bundles numbered 1, 2 and 3 with hollow tube of vessels V_1 and V_2, see Fig. 4. These models are then imported to the FEA software to form cubic RVEs having a size of 1 mm × 1 mm × 1 mm ($L \times W \times t$) for all layers, except the outer layer which have a width (W) of 0.6 mm to ensure achieving the required fiber volume fraction. These computed fibrous and tube vessel areas for each layer are listed in Table 2.

The orthotropic nature of Moso bamboo can be described by an accurate estimate of the nine material constants at three principal directions: three elastic moduli, three Poisson's ratios and three shear moduli. To accommodate for the effect of geometrical variations of bamboo constituents at the micro-scale, a finite element based numerical RVE homogenisation approach is used [28,36,47]. The anatomy-based RVEs were analysed using the EasyPBCs homogenisation tool in ABAQUS FEA software using hexahedral element shape with structured meshing technique. Three-dimensional 20-node quadratic brick elements with reduced integration method (C3D20R) are adopted. After sensitivity analysis for mesh sizes ranging from 0.02 to 0.06 mm, see Supplementary Material B for the complete analysis, the applied mesh size of 0.03 mm is chosen which gives acceptable results while being efficient from a time and memory-saving point of view. The number of elements are 45276, 50853, 46,893 and 28611, from the inner to the outer layers, respectively.

5. Results and comparisons with experiments

In this section, we compare the homogenised elastic properties to experimental data available in the literature from tensile tests of Moso bamboo strips [19]. In particular, we concentrate on the elastic modulus E_{11} of strips taken from inner towards outer layers. The effective elastic properties of Moso bamboo microstructure are estimated theoretically using four analytical homogenisation models, namely, IROM, H-T, M−T and Chamis with the inputs of elastic properties given in Table 1. The state-of-the-art single-fibre RVE and our anatomy-based numerical simulations are also applied to obtain numerical homogenisation.

Table 3 summarises the results obtained by the four analytical methods and by the two numerical RVE based homogenisation methods along with the available experimental data. The results, in general, show that the elastic modulus E_{11} along the longitudinal direction is predictable and proportional to the volume fraction of bamboo fibres, which is consistent with previous experimental and analytical studies [20,27,48] as well as with a recent numerical study [28]. This means that the longitudinal behavior of bamboo is dominated by fibre properties. It is worth mentioning that the results of the analytical methods and of the single fibre based numerical RVE show higher overall material properties than those obtained from the anatomy-based RVE. It is attributed to the fact that the former models are transversely isotropic, contrary to real bamboo microstructure. The reason behind this is that the former models simplify the actual geometrical variations of bamboo microstructure and hence the applied boundary uniform tractions on different fibre bundles will incur different strains [14].

5.1. Young's moduli E_{11}, E_{22} and E_{33}

Fig. 5 shows the comparison of the elastic modulus obtained by the analytical and numerical methods detailed above. The axial elastic modulus E_{11}, refer to Fig. 5a, at the outer and middle-2 layers obtained from analytical homogenisation and single fibre numerical RVEs differ by up to 3.6 % compared to the experimental data. However, for the middle-1 and inner layers, the results of analytical homogenisation and single fibre numerical RVEs match very well. In contrast, the numerical results of the anatomy-based RVE homogenisation give excellent predictions at the outer and middle-2 layers as well. This is due to the accurate representation of constituents (including vessels) and the morphological shape of bamboo fibres. Note that for a higher volume fraction of fibre, the stiffer phase has a more pronounced contribution to the stiffness of the RVE.

For the elastic modulus in the radial and tangential directions, E_{22} and E_{33}, respectively (Fig. 5b and c), the anatomy-based RVE results lie between the analytical upper and lower bounds. Mori-Tanaka and Halpin-Tsai analytical models show good agreement with both numerical single fibre RVE and anatomy-based RVE homogenisation results in the inner, middle-1 and middle-2 layers, while the results of E_{33} differ greatly in the outer layer. This is not surprising as both M−T and H-T have been proved to give higher accuracy in the radial and tangential directions based on the research conducted by Zhao et al. [26].

Our anatomy-based RVE model shows anisotropy in the transverse directions. This manifests itself in different elastic moduli E_{22} and E_{33}. In this respect, the anatomy-based RVE model is capable of capturing the inherent transverse anisotropy of Moso bamboo.

5.2. Shear moduli G_{12}, G_{13} and G_{23}

For the shear moduli G_{12} and G_{13} (see Fig. 6a and b), both the analytical (M−T and H-T) and numerical single fibre and anatomy-based RVE homogenisation results agree very well at lower volume fractions in the inner and middle-1 layers. However, a larger variation of shear stiffness is visible at higher volume fractions in the middle-2 and outer

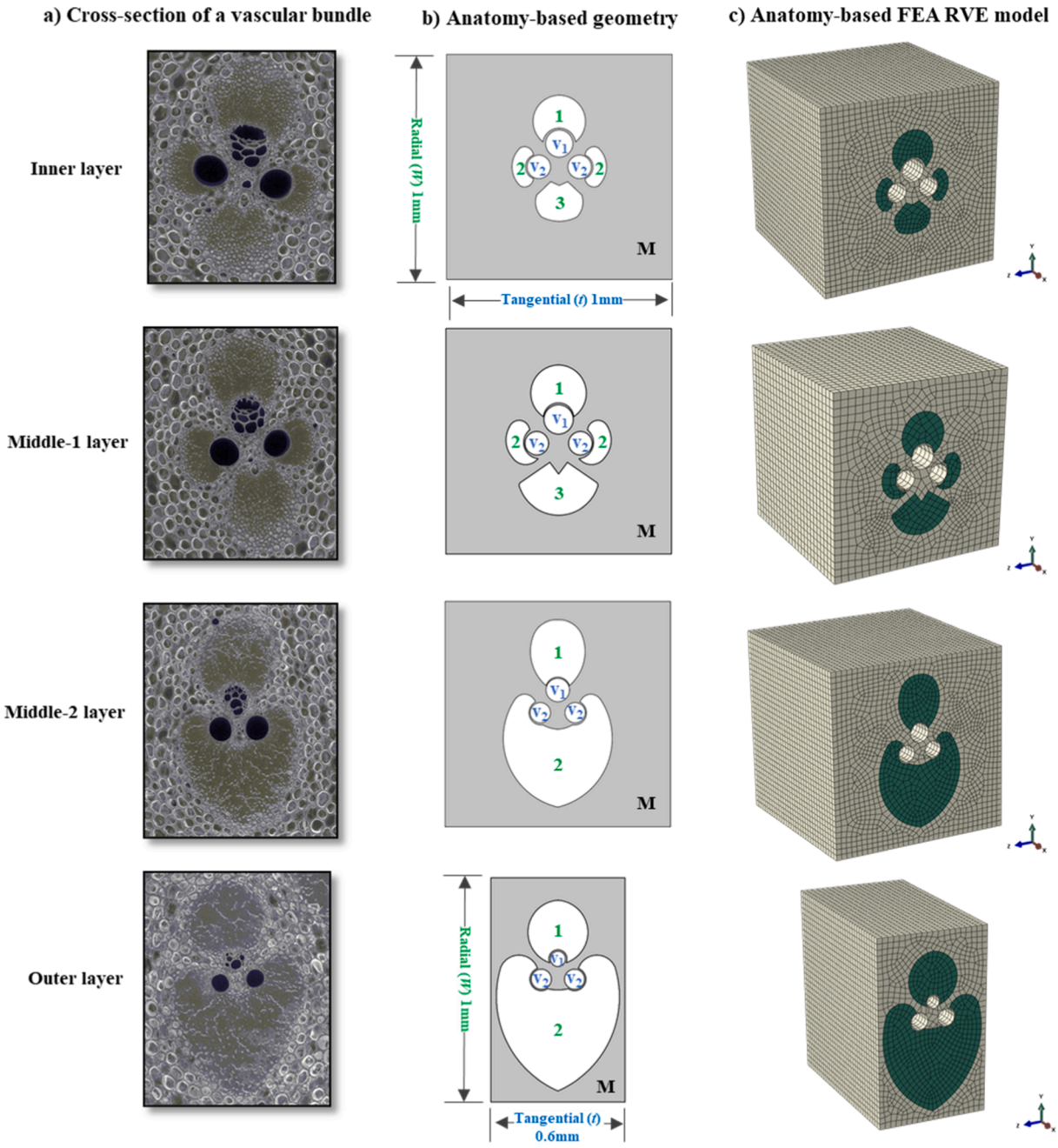

Fig. 4. An illustration of: a) Cross-section of a vascular bundle (reproduced from [9]). b) Simplified, anatomy-based geometry of the vascular bundle including the fibre bundles 1, 2, and 3, matrix M, and hollow tube vessels V_1 and V_2. (c) Corresponding FEA RVE models. The rows from top to bottom correspond to inner, middle-1, middle-2 and outer layers of the bamboo culm.

Table 2
Average areas of bamboo fibre bundles and tube vessels.

Layers	Inner	Middle-1	Middle-2	Outer
Fibre volume fraction(V_f)	8.53%	12.69%	21.86%	47.2%
A_1(mm^2)	0.0334	0.040	0.0555	0.0597
A_2(mm^2)	0.0114	0.0158	0.0163	0.2241
A_3(mm^2)	0.0291	0.0553	–	–
V_1(mm^2)	0.0114	0.0134	0.0086	0.0053
V_2(mm^2)	0.0086	0.0106	0.0060	0.0033

layers. For shear modulus G_{23} (see Fig. 6c), the obtained values show good agreement of the M−T, H-T, of the single fibre RVE and of the anatomy-based RVE models. Note, however, that the Chamis model overestimates the shear moduli.

We observe in Fig. 6 that shear moduli G_{12} and G_{13} obtained from the analytical homogenisation and from single fibre RVE are the same. However, these moduli are different as obtained from the anatomy-based RVE. This is the consequence of the fact that the anatomy-based RVE model captures the real geometry of fibre bundles and has its transversal anisotropy. Note that the analytical homogenisation methods such as H-T have only a curve fitting parameter to account for the fibre geometry, the microstructure alignment and the loading conditions [26].

Table 3
Estimated elastic constants for Moso bamboo and numerical RVE's with gradient volume fractions. The experimental data is obtained from Ref. [19].

Engineering constants	Young's modulus (GPa)			Poisson's ratio			Shear modulus (GPa)		
	E_{11}	E_{22}	E_{33}	ν_{12}	ν_{13}	ν_{23}	G_{12}	G_{13}	G_{23}
Outer layer	Fibre volume fraction = 47.20%								
IROM	31.395	5.745	5.745	0.32	0.32	0.42	–	–	–
M-T	31.393	5.37	5.37	0.30	0.30	0.44	2.085	2.085	1.858
H-T	31.39	6.994	6.994	0.31	0.31	0.44	2.085	2.085	1.858
Chamis	31.39	6.426	6.426	0.31	0.31	0.44	2.405	2.405	2.405
Single fibre-RVE	31.408	6.593	6.593	0.30	0.30	0.32	2.118	2.118	1.606
Anatomy-RVE	31.272	6.417	8.472	0.30	0.30	0.26	2.201	2.920	1.850
Experimental	30.30	–	–	–	–	–	–	–	–
Mid-layer 2	Fibre volume fraction = 21.86%								
IROM	14.370	3.820	3.820	0.34	0.34	0.43	–	–	–
M-T	14.281	3.328	3.328	0.32	0.32	0.45	1.217	1.217	1.143
H-T	14.281	3.736	3.736	0.32	0.32	0.45	1.217	1.217	1.143
Chamis	14.279	3.927	3.927	0.32	0.32	0.45	1.467	1.467	1.467
Single fibre-RVE	14.287	3.494	3.494	0.32	0.32	0.43	1.218	1.218	1.090
Anatomy-RVE	14.229	3.694	3.534	0.31	0.32	0.41	1.377	1.188	1.095
Experimental	14.20	–	–	–	–	–	–	–	–
Mid-layer 1	Fibre volume fraction = 12.69%								
IROM	8.938	3.291	3.291	0.34	0.34	0.44	–	–	–
M-T	8.933	2.846	2.846	0.33	0.33	0.44	1.021	1.021	0.982
H-T	8.932	2.986	2.986	0.33	0.33	0.44	1.021	1.021	0.982
Chamis	8.932	3.284	3.284	0.33	0.33	0.44	1.226	1.226	1.226
Single fibre-RVE	8.937	2.894	2.894	0.33	0.33	0.44	1.021	1.021	0.964
Anatomy-RVE	8.868	2.722	2.776	0.32	0.32	0.44	1.050	1.022	0.970
Experimental	8.93	–	–	–	–	–	–	–	–
Inner Layer	Fibre volume fraction = 8.53%								
IROM	6.6037	3.026	3.026	0.34	0.34	0.43	–	–	–
M-T	6.599	2.644	2.644	0.33	0.33	0.43	0.944	0.944	0.919
H-T	6.598	2.691	2.691	0.33	0.33	0.43	0.944	0.944	0.919
Chamis	6.598	3.001	3.001	0.33	0.33	0.43	1.12	1.12	1.12
Single fibre-RVE	6.601	2.665	2.665	0.33	0.33	0.43	0.944	0.944	0.911
Anatomy-RVE	6.54	2.51	2.553	0.33	0.33	0.43	0.949	0.931	0.898
Experimental	6.65	–	–	–	–	–	–	–	–

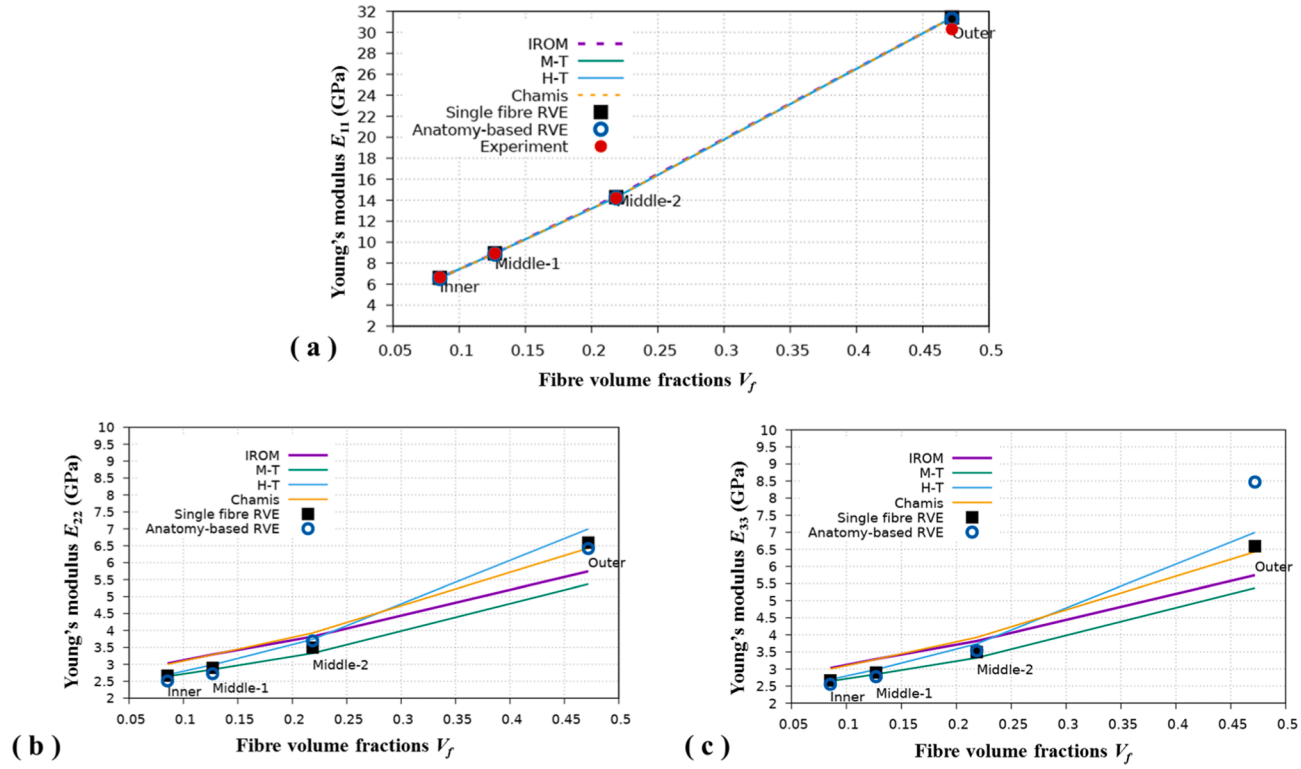

Fig. 5. Effective Young's moduli of Moso bamboo in the (a) axial E_{11}, (b) radial E_{22}, and (c) tangential E_{33} directions as a function of fibre contents. The experimental data are taken from tensile coupon measurements [19] of 11–13 Moso bamboo internodes aged four 4 years.

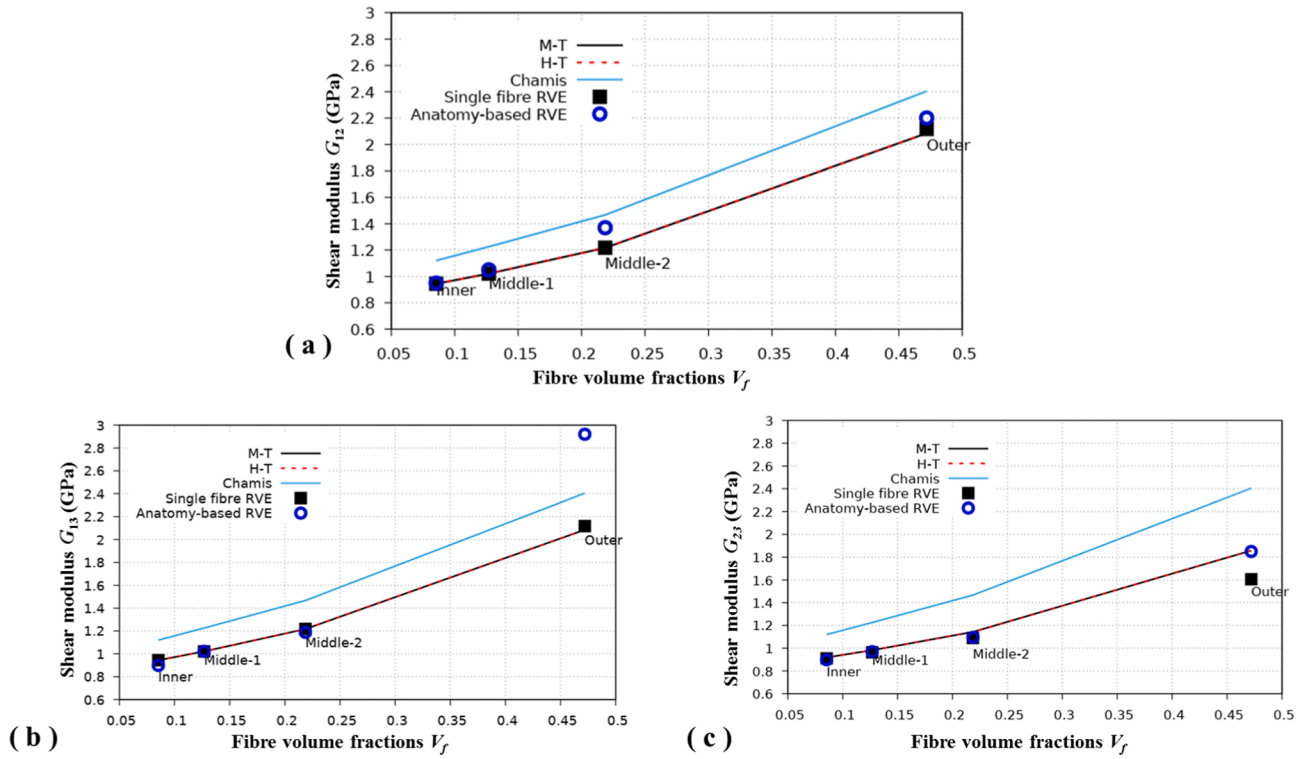

Fig. 6. Effective shear moduli of Moso bamboo (a) G_{12}, (b) G_{13} and (c) G_{23} as a function of fibre volume fraction obtained with different models.

5.3. *Poisson's ratios v_{12}, v_{13} and v_{23}*

For Poisson's ratio v_{12} and v_{13} (see Fig. 7a and b), again, the results from M−T and H-T analytical models and those from the numerical single fibre RVE are close in all layers. The predictions of the anatomy-based RVE are close to them in the inner and outer layers, while the estimation is slightly lower at the middle-1 and 2 layers. This is explained by the transverse anisotropy of the anatomy-based RVE, in accordance to the same property of real bamboo. When traction is applied along the longitudinal axis, the RVE deforms along the

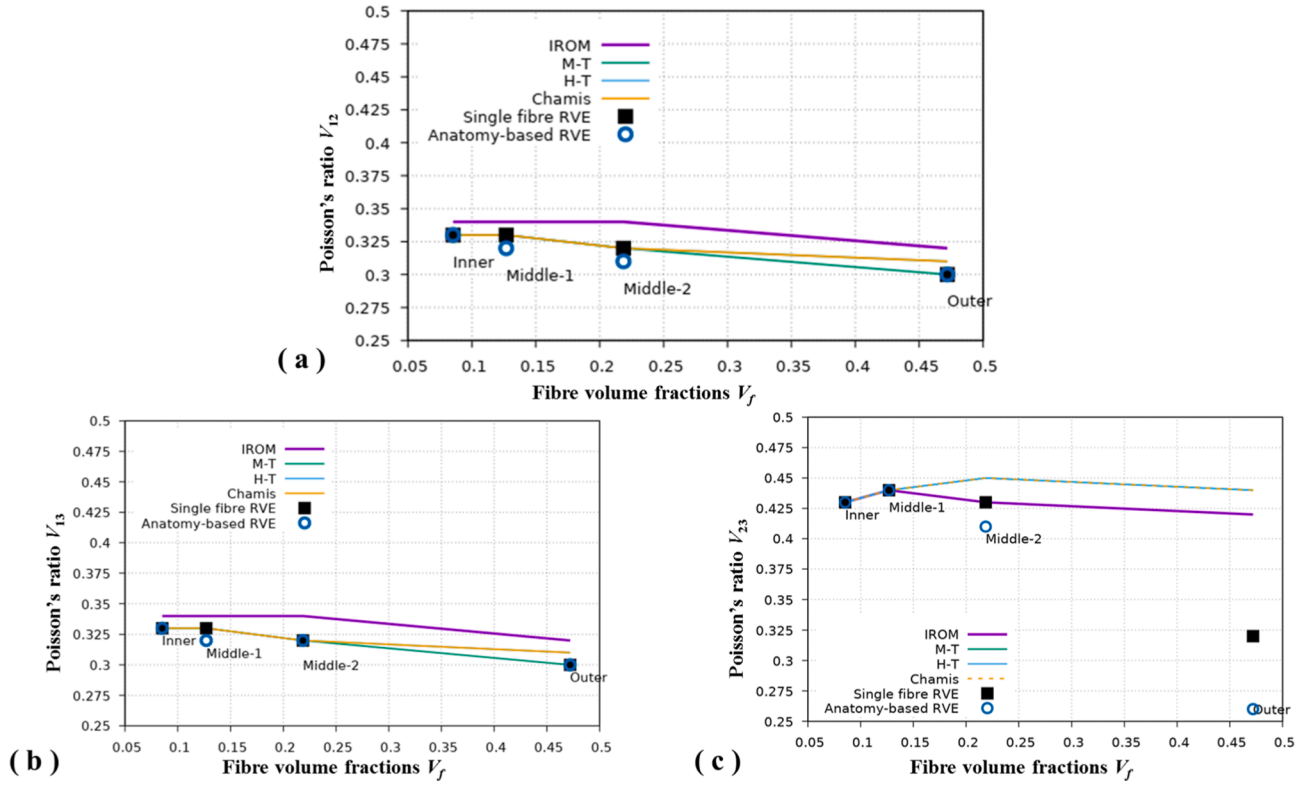

Fig. 7. Effective Poisson's ratios of Moso bamboo (a) v_{12}, (b) v_{13} and (c) v_{23} as a function of fibre voluma fraction obtained from different models.

directions transversal to the applied traction, implying strains at both the radial and the tangential directions. The analytical models and single fibre RVE simplify the actual geometrical variations of bamboo microstructure, and are unable to account for the different strains in the transversal directions. In other words, their behaviour is transversely isotropic. Contrary, our anatomy-based RVE is anisotropic the fibre bundles forming the vascular bundles mimic the real geometry. As a consequence, the uniform tractions applied on the boundary of the different fibre bundles incur different strains [14] that result in different Poisson's ratios in the radial and tangential directions.

Poisson's ratio v_{23} (see Fig. 7c) obtained from the predictions of M−T and H-T models and those of the numerical single fibre RVE have similar trends; they match in all layers except at the outer ones. The anatomy-based RVE and single fibre RVE estimations are closer to each other at lower volume fractions in the inner, middle-1 and middle-2 layers, while they deviate at high volume fractions in the outer layer. It is worth noting that predictions from IROM are higher than those obtained from all other models for Poisson's ratios v_{12} and v_{13}, while the predictions of IROM for v_{23} are closer to M−T and single fibre RVE.

5.4. Material properties and the elastic strain energy

To shed more light on the cause of the deviation between the results obtained from the numerical single fibre RVE and the anatomy-based RVE, we compute the elastic strain energy stored in the fibres and in the matrix [50]. The elastic strain energy stored in the RVE can be computed by integrating the product of the stresses and strains in the elastic regime as:

$$\bar{U} = \frac{1}{2}\int_V \bar{\bar{\sigma}}\bar{\bar{\varepsilon}} dV \tag{18}$$

where $\bar{U}$ is the elastic strain energy stored in the RVE and dV is the volume of the RVE.

In order to gain insight into how the load is distributed between the fibres and the matrix, we compute the ratio of $\bar{U}$ in the fibres to that in the matrix indicating the distribution of internal strains in the RVE. Here we show results for the middle-2 layer as their anatomy-based RVE provides an E_{11} perfectly matching with that observed in experiment.

As we have seen in Fig. 5a, stiffness modulus E_{11} for a single fibre RVE differs from that for the anatomy-based RVE by about 0.4%. This is in accordance with a small difference between the ratios of the strain energy $\bar{U}$ in the fibre to that in the matrix in case of the single fibre and the anatomy-based RVE models. As shown in Fig. 8a, in case of the traction used to measure E_{11} we find a ratio of 7.45 in case of the single fibre RVE compared with 7.65 for the anatomy-based RVE. These small deviations mean that E_{11} is not very sensitive to fibre morphology.

This deviation is more characteristic in the case of Young's moduli E_{22} and E_{33}. As we have seen in Fig. 5b and c, E22 and E33 measured from the single fibre and from the anatomy-based RVE model differ by 5.4% and 1.1%, respectively, the single fibre RVE model predicts lower stiffness. This is explained by the ratio of strain energy $\bar{U}$ in the fibres to that of the matrix. In the case of the single fibre RVE, this ratio is 0.053 for both E22 and E33, whereas in the anatomy-based RVE the ratio is 0.1 (for E_{22}) and 0.084 (for E_{33}), see Fig. 8b. The significantly higher ratio of elastic strain energy reflects that the fibres carry a larger part of the load in the anatomy-based model. Hence resistance of bamboo fibres is found to be higher in the anatomy-based RVE model, leading to higher overall E_{22} and E_{33} stiffness.

We have seen in Fig. 6 that the shear moduli obtained from the anatomy-based RVE model are higher than those obtained from the single fibre RVE model. Fig. 6a shows the largest difference of about 1.3 % in G_{12}. This difference can be attributed to the higher stresses in the fibres that are also stiffer than the matrix, hence the anatomy-based model, capturing the true morphology of fibres and vessels, gives higher overall stiffness. This observation is confirmed in Fig. 9, which shows the strain energy in the fibres and the matrix for both models. Fig. 9a also shows the ratio of the elastic strain energy $\bar{U}$ in the fibres to that in the matrix in case of G_{12} and G_{13}. For G_{12}, this ratio is 0.072 for

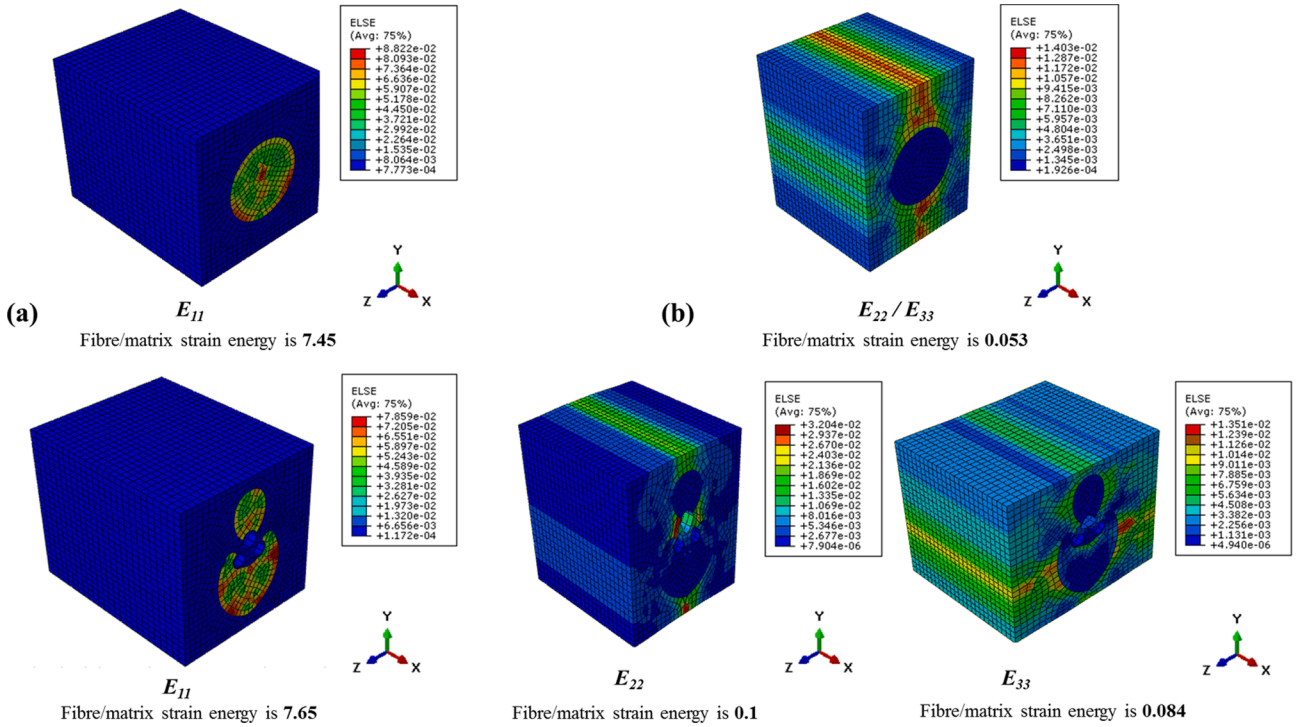

Fig. 8. Colour coding shows the strain energy in each finite element in the fibres and in the matrix during traction used to compute the effective Young's moduli in the middle-2 layer. (a) E_{11} in case of the single fibre RVE (upper) and anatomy-based RVE (lower), (b) E_{22} (radial) and E_{33} (tangential) moduli in case of the single fibre RVE (upper) and anatomy-based RVE (lower images). The ratio of the elastic strain energy in the fibres to that in the matrix is also indicated.

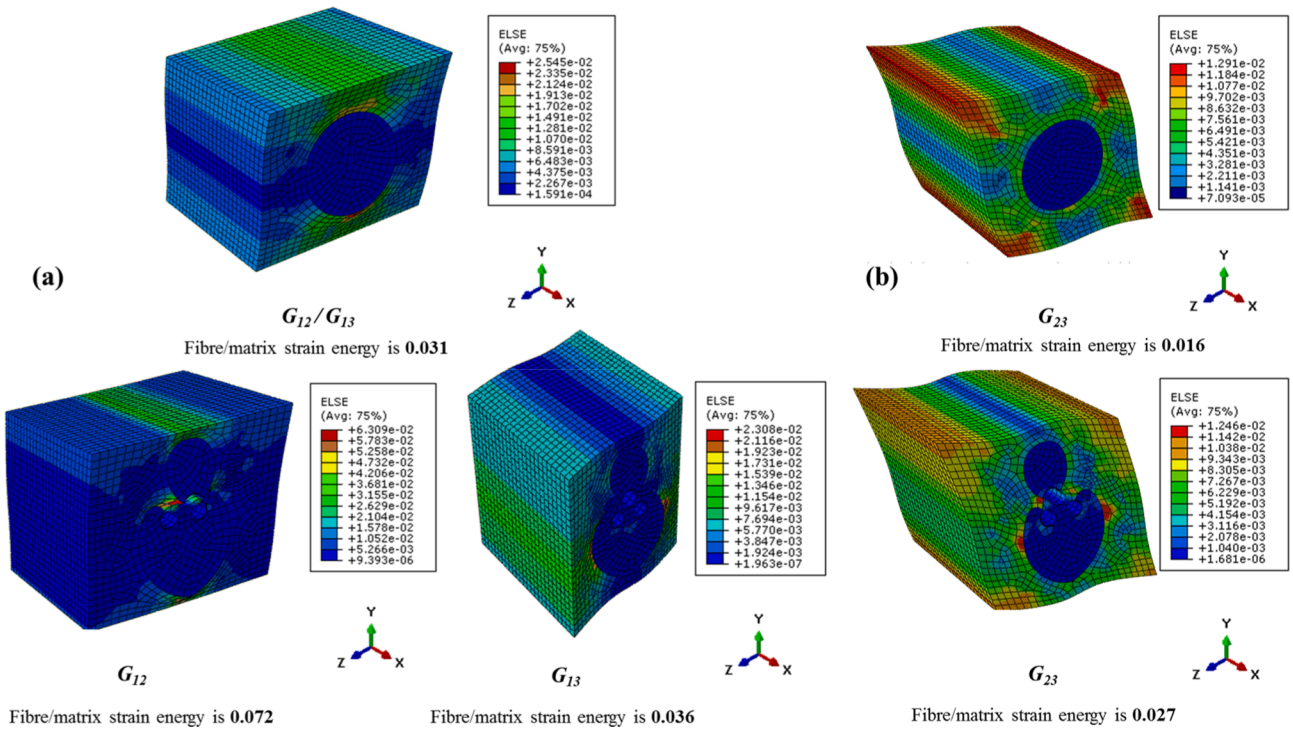

Fig. 9. Colour coding shows the strain energy in each finite element in the fibres and in the matrix during traction used to compute the effective shear moduli in the middle-2 layer. (a) G_{12} and G_{13} in case of the single fibre RVE (upper) and anatomy-based RVE (lower), (b) G_{23} in case of the single fibre RVE (upper) and anatomy-based RVE (lower image). The ratio of the elastic strain energy in the fibres to that in the matrix is also indicated.

the anatomy-based RVE compared with 0.031, that for the single fibre RVE. This indicates that fibres are resisting more the applied shear strains than the matrix in the anatomy-based RVE model. These observations also hold for G_{13}, see Fig. 6b and 9a. In particular, Fig. 9a shows higher fibre to matrix strain energy ratio of 0.036 for the anatomy-based RVE model as compared with that of the single fibre RVE model, which gives 0.031. Similarly, G_{23} (see Fig. 6c) is also lower in single fibre RVE compared to the anatomy-based RVE. This also manifests itself in lower fibre to matrix strain energy ratio in case of the single fibre RVE model (0.016), as compared with that in case of the anatomy-based RVE model (0.027), see Fig. 9b.

6. Conclusions and future work

In this study, the effective elastic properties of Moso bamboo (Phyllostachys edulis) microstructure are estimated using four analytical homogenisation models (namely, IROM, H-T, M−T and Chamis) and the state-of-the-art numerical single-fibre RVE homogenisation. These models consider the material to be transversely isotropic. But in reality, bamboo has an anisotropic structure with different elastic properties in each lateral direction due to the complex microstructure of the material. To account for this microstructure, this study introduces a novel anatomy-based RVE homogenisation model, which is compared and validate against methods mentioned earlier.

The numerical simulations of the anatomy-based RVE model are based on a reconstruction of selected scanning electron microscopy images of bamboo internodes from the literature [10]. The effective elastic properties of the anatomy-based RVE are then obtained using the FEA software. The results obtained from numerical RVE models, analytical models, and available experimental data are compared. Based on the results obtained from this study, the following can be concluded:

- The elastic strain energy ratio between the fibre and matrix phase is used to investigate the variations in the effective elastic properties for the single-fibre and anatomy-based RVEs.
- The homogenised Young's modulus E_{11} obtained from the anatomy-based RVE model shows good accuracy to experimental data.
- Young's modulus E_{11} is not sensitive to fibre shape variations. However, transversal Young's moduli E_{22} and E_{33} are sensitive to actual fibre geometry due to the inherent transversal anisotropy of bamboo material.
- Shear moduli G_{12}, G_{13} G_{23} are sensitive to fibre cluster geometry. This is also a consequence of the transversal anisotropy of bamboo and of the anatomy-based RVE model.

Based on the above, it was concluded that the proposed anatomy-based RVE model is capable of capturing the transversal anisotropy of bamboo's microstructure. This enabled estimating the transversal properties of bamboo playing an important role in bamboo mechanical behaviour. This underlines the need to conduct orthotropic modelling for bamboo to interpret experimental results, which is emphasised by Akinbade and Harries [49]. However, it is clear that to fully uncover the effects of orthotropic modelling further work is required. This effort can be support by the application of the elastic strain energy ratio which provides information on the anisotropy of the material properties. These considerations are suggested to pursue as the next steps.

The findings of this study can also be compared with those presented by Akinbade et al [22], where the gradient in the transverse material properties are shown to be supported by the morphology of its components. Therefore, accounting for the anatomy-based details is very important to capture the intricate behaviour of bamboo structures.

To conclude, the developed autonomy-based RVE offers the possibility to understand the effect of geometrical variation in bamboo. The utilisation of autonomy-based RVE is not restricted to bamboo, as it can be used in other natural materials such as wood, bone, and chitin. The anatomy based RVE method eliminates the need for strict assumptions such as those used in analytical solutions, and relies on a detailed description of the micro-level of bamboo or other materials. In the following steps, the authors expect to extend the study of anatomy-based RVE homogenisation beyond the elastic phase and to develop extended

models to elucidate the thermal and moisture content effects.

CRediT authorship contribution statement

Layth S. Al-Rukaibawi: Conceptualization, Methodology, Writing - original draft, Software, Formal analysis, Validation, Resources. **Sadik L. Omairey:** Conceptualization, Writing - review & editing. **György Károlyi:** Writing - review & editing, Supervision, Funding acquisition.

Declaration of Competing Interest

The authors declare that they have no known competing financial interests or personal relationships that could have appeared to influence the work reported in this paper.

Acknowledgements

This work was supported by the Hungarian NKFIH under grant No. K-128584 and by the NRDI Funds BME IES-VIZ TKP2020 and TKP2021-NVA BME. L S A-R was supported by the Stipendium Hungaricum scholarship scheme.

Appendix A. Supplementary data

Supplementary data to this article can be found online at https://doi.org/10.1016/j.conbuildmat.2021.125036.

References

[1] A. Det Udomsap, P. Hallinger, A bibliometric review of research on sustainable construction, 1994–2018, J. Clean. Prod. 254 (2020) 120073. 10.1016/j.jclepro.2020.120073.
[2] D. Farrelly, The book of bamboo: a comprehensive guide to this remarkable plant, its uses, and its history, Thames and Hudson Ltd, London, 1996.
[3] M. Mahdavi, P.L. Clouston, S.R. Arwade, A low-technology approach toward fabrication of laminated bamboo lumber, Constr. Build. Mater. 29 (2012) 257–262, https://doi.org/10.1016/j.conbuildmat.2011.10.046.
[4] V. Der Lugt, Pablo.,, Booming bamboo: the (re) discovery of a sustainable material with endless possibilities, 1st Ed.,, Jeroen van Oostveen, 2017.
[5] M. Ahmad, F.A. Kamke, Analysis of Calcutta bamboo for structural composite materials: physical and mechanical properties, Wood Sci. Technol. 39 (6) (2005) 448–459.
[6] S. Amada, Sun Untao, Fracture properties of bamboo, Compos. Part B Eng. 32 (5) (2001) 451–459, https://doi.org/10.1016/S1359-8368(01)00022-1.
[7] W. Liese, The anatomy of bamboo culms, Brill (1998).
[8] X. Londoño, G.C. Camayo, N.M. Riaño, Y. López, Characterization of the anatomy of Guadua angustifolia (Poaceae: Bambusoideae) culms, Bamboo Sci, Cult. J. Am. Bamboo Soc. 16 (2002) 18–31.
[9] P. G. Dixon and L. J. Gibson, Sample of the Data Generated in the Structural Bamboo Project of the Cellular Solids Group (at MIT), DSpace@MIT. (2014). https://dspace.mit.edu/handle/1721.1/88182 (accessed January 20, 2021).
[10] P.G. Dixon, L.J. Gibson, The structure and mechanics of Moso bamboo material, J. R. Soc. Interface. 11 (2014), https://doi.org/10.1098/rsif.2014.0321.
[11] T.Y Lo, H.Z Cui, H.C Leung, The effect of fiber density on strength capacity of bamboo, Mater. Lett. 58 (21) (2004) 2595–2598.
[12] L. Huanrong, Study on the properties and mechanism of fracture in bamboo (Ph.D. dissertation), China Knowledge Network (CNKI) (2010).
[13] Z.P. Shao, C.H. Fang, S.X. Huang, G.L. Tian, Tensile properties of Moso bamboo (Phyllostachys pubescens) and its components with respect to its fiber-reinforced composite structure, Wood Sci. Technol. (2010), https://doi.org/10.1007/s00226-009-0290-1.
[14] H. Li, S. Shen, The mechanical properties of bamboo and vascular bundles, J. Mater. Res. 26 (21) (2011) 2749–2756, https://doi.org/10.1557/jmr.2011.314.
[15] J.F. Correal D.J. Arbeláez, Influence of age and height position on colombian guadua angustifolia bamboo mechanical propertieS, Maderas. Cienc. y Tecnol. 12 (2010) 105–113. 10.4067/S0718-221X2010000200005.
[16] T. Tan, N. Rahbar, S.M. Allameh, S. Kwofie, D. Dissmore, K. Ghavami, W. O. Soboyejo, Mechanical properties of functionally graded hierarchical bamboo structures, Acta Biomater. 7 (10) (2011) 3796–3803, https://doi.org/10.1016/j.actbio.2011.06.008.
[17] J.J. García, C. Rangel, K. Ghavami, Experiments with rings to determine the anisotropic elastic constants of bamboo, Constr. Build. Mater. (2012), https://doi.org/10.1016/j.conbuildmat.2011.12.089.
[18] B. Sharma, K.A. Harries, K. Ghavami, Methods of determining transverse mechanical properties of full-culm bamboo, Constr. Build. Mater. (2013), https://doi.org/10.1016/j.conbuildmat.2012.07.116.
[19] H. Liu, Z. Jiang, X. Zhang, X. Liu, Z. Sun, Effect of fiber on tensile properties of moso bamboo, BioResources. 9 (2014) 6888–6898. 10.15376/biores.9.4.6888-6898.
[20] L. Shang, Z. Sun, X. Liu, Z. Jiang, A novel method for measuring mechanical properties of vascular bundles in moso bamboo, J. Wood Sci. 61 (6) (2015) 562–568, https://doi.org/10.1007/s10086-015-1510-y.
[21] K.A. Harries, J. Bumstead, M. Richard, D. Trujillo, Geometric and material effects on bamboo buckling behaviour, Proc. Inst. Civ. Eng. - Struct. Build. 170 (4) (2017) 236–249, https://doi.org/10.1680/jstbu.16.00018.
[22] Y. Akinbade, K.A. Harries, C.V. Flower, I. Nettleship, C. Papadopoulos, S. Platt, Through-culm wall mechanical behaviour of bamboo, Constr. Build. Mater. 216 (2019) 485–495, https://doi.org/10.1016/j.conbuildmat.2019.04.214.
[23] M.G. Gonzalez, J. Madden, C. Maluk, Experimental study on compressive and tensile strength of bamboo at elevated temperatures, in: World Conf. Timber Eng. August, 2018: pp. 20–23.
[24] P.H. Lee, M. Odlin, H. Yin, Development of a hollow cylinder test for the elastic modulus distribution and the ultimate strength of bamboo, Constr. Build. Mater. (2014), https://doi.org/10.1016/j.conbuildmat.2013.10.051.
[25] Y.Z. Wang, C.L. Zhang, W.Q. Chen, An analytical model to predict material gradient and anisotropy in bamboo, Acta Mech. (2017), https://doi.org/10.1007/s00707-015-1514-0.
[26] X. Zhao, G. Wang, Y. Wang, Micromechanical modeling in determining the transverse elastic moduli and stress distributions of bamboo, J. Mater. Sci. 53 (4) (2018) 2553–2565, https://doi.org/10.1007/s10853-017-1692-3.
[27] E.C.N. Silva, M.C. Walters, G.H. Paulino, Modeling bamboo as a functionally graded material: Lessons for the analysis of affordable materials, J. Mater. Sci. 41 (2006) 6991–7004, https://doi.org/10.1007/s10853-006-0232-3.
[28] J. Cui, Z. Qin, A. Masic, M.J. Buehler, Multiscale structural insights of load bearing bamboo: a computational modeling approach, J. Mech. Behav. Biomed. Mater. 107 (2020) 103743, https://doi.org/10.1016/j.jmbbm.2020.103743.
[29] L. Osorio, E. Trujillo, F. Lens, J. Ivens, I. Verpoest, A.W. Van Vuure, In-depth study of the microstructure of bamboo fibres and their relation to the mechanical properties, J. Reinf. Plast. Compos. 37 (17) (2018) 1099–1113, https://doi.org/10.1177/0731684418783055.
[30] M.D.E. Candelaria, J.Y. Hernandez Jr, Determination of the properties of bambusa blumeana using full-culm compression tests and layered tensile tests for finite element model simulation using orthotropic material modeling, ASEAN Eng. J. 9 (2019) 54–71.
[31] A. Zhou, D. Huang, H. Li, Y. Su, Hybrid approach to determine the mechanical parameters of fibers and matrixes of bamboo, Constr. Build. Mater. (2012), https://doi.org/10.1016/j.conbuildmat.2012.03.011.
[32] W. Voigt, Ueber die Beziehung zwischen den beiden Elasticitätsconstanten isotroper Körper, Ann. Phys. (1889), https://doi.org/10.1002/andp.18892741206.
[33] A. Reuss, Calculation of the centrifugal limit of mixed crystals due to the plasticity condition for single crystals, Z. Angew. Math. Mech. 9 (1929) 49–58.
[34] H. Qing, L. Mishnaevsky, 3D multiscale micromechanical model of wood: from annual rings to microfibrils, Int. J. Solids Struct. 47 (9) (2010) 1253–1267, https://doi.org/10.1016/j.ijsolstr.2010.01.014.
[35] R. Hill, Theory of mechanical properties of fibre-strengthened materials-III. self-consistent model, J. Mech. Phys. Solids. (1965), https://doi.org/10.1016/0022-5096(65)90008-6.
[36] R.L. Hewitt, M.C. De Malherbe, An approximation for the longitudinal shear modulus of continuous fibre composites, J. Compos. Mater. 4 (2) (1970) 280–282, https://doi.org/10.1177/002199837000400214.
[37] C.C. Chamis, Mechanics of composite materials: past, present, and future, J. Compos. Technol. Res. (1989), https://doi.org/10.1520/ctr10143j.
[38] H. Hosseini, R. Kolahchi, M.M. Heydari, Elastic analysis of polymeric cylinders reinforced with carbon nanotubes, J. Appl. Math. Comput. Mech. 15 (2016) 31–39. 10.17512/jamcm.2016.2.04.
[39] D.T. Luther, Homogenisation of damaged concrete meso-structures using representative volume elements–implementation and application to slang, Weimar Ger, Bauhaus-University. (2005).
[40] L. Wu, C.N. Chung, Z. Major, L. Adam, L. Noels, From SEM images to elastic responses: A stochastic multiscale analysis of UD fiber reinforced composites, Compos. Struct. (2018), https://doi.org/10.1016/j.compstruct.2018.01.051.
[41] A.J. Sobey, J.I.R. Blake, R.A. Shenoi, Reliability of composite marine structures, in: Durab. Compos. a Mar. Environ. 2, Springer, 2018: pp. 113–134.
[42] Z. Xia, Y. Zhang, F. Ellyin, A unified periodical boundary conditions for representative volume elements of composites and applications, Int. J. Solids Struct. 40 (8) (2003) 1907–1921, https://doi.org/10.1016/S0020-7683(03)00024-6.
[43] S.L. Omairey, P.D. Dunning, S. Sriramula, Development of an ABAQUS plugin tool for periodic RVE homogenisation, Eng. Comput. 35 (2) (2019) 567–577, https://doi.org/10.1007/s00366-018-0616-4.
[44] R. Hill, Elastic properties of reinforced solids: some theoretical principles, J. Mech. Phys. Solids. (1963), https://doi.org/10.1016/0022-5096(63)90036-X.
[45] A.K. Ray, S.K. Das, S. Mondal, P. Ramachandrarao, Microstructural characterisation of bamboo, J. Mater. Sci. 39 (2004) 1055–1060.

[46] S. Amada, Y. Ichikawa, T. Munekata, Y. Nagase, H. Shimizu, Fiber texture and mechanical graded structure of bamboo, Compos. Part B Eng. 28 (1-2) (1997) 13–20.
[47] Z. Shao, F. Wang, Modeling on the Toughness Fracture and Energy-Absorbing Mechanism of Biomaterial—Bamboo (Phyllostachys pubescens), in: Fract. Mech. Plant Mater., Springer, 2018: pp. 199–221.
[48] R. de Medeiros, M.E. Moreno, F.D. Marques, V. Tita, Effective properties evaluation for smart composite materials, J. Brazilian Soc. Mech. Sci. Eng. (2012), https://doi.org/10.1590/S1678-58782012000500004.
[49] Y. Akinbade, K.A. Harries, Is the rule of mixture appropriate for assessing bamboo material properties? Constr. Build. Mater. 267 (2021), 120955 https://doi.org/10.1016/j.conbuildmat.2020.120955.
[50] M.H. Sadd, Strain energy and related principles, Elast. (Third Ed. Theory, Appl. Numer. (2014) 119–139.